Austrian Journal of Earth Sciences | Vienna | 2015 | Volume 108/2 | 209 - 218 | DOI: 10.17738/ajes.2015.0022

Earthquake interactions during the 2013 Ebreichsdorf aftershock sequence

Jean Baptiste TARY[1)2)], Maria-Theresia APOLONER[1)] & Götz BOKELMANN[1)*)]

[1)] Department of Meteorology and Geophysics, University of Vienna, Althanstrasse 14, 1090 Wien, Austria;

[2)] Department of Physics, University of Alberta, 8440 - 112 St, Edmonton, Alberta T6G 2R7, Canada;

[*)] Corresponding author, goetz.bokelmann@univie.ac.at

KEYWORDS Earthquake interactions; Stress transfer; Vienna Basin; Eastern Alps

Abstract

The Vienna Basin Fault System (VBFS) is one of the most seismically active regions of Austria, delineating the southern part of the Vienna Basin. This sinistral, strike slip fault system, accommodates part of the deformation due to the northward push of the Adriatic microplate. In 2000 and 2013, two pairs of main shocks followed by a few tens of aftershocks occurred in the region of Ebreichsdorf, one of the clusters of seismicity along the VBFS. The main shocks seem to be located closely in both cases, even though high-resolution double-difference locations are available only for the sequence in 2013. Focusing on this sequence, we investigate the interactions between the two main shocks and their 18 aftershocks. The two main shocks are located almost at the same place, at a depth of 10.5 km, while the aftershocks constitute a shallower ellipsoid with its long axis parallel to the main trace of the VBFS. We use two Coulomb failure stress models to study possible static stress transfer between the main shocks and the aftershocks of this sequence, the apparent friction model and the isotropic poroelastic model. Both models yield Coulomb failure stress changes below 0.01 MPa at the aftershocks locations. Static stress transfer seems then unlikely to explain their occurrence, even though interactions between aftershocks could play a role in their triggering. Two other mechanisms are considered, namely pore pressure diffusion along an idealized fault plane, and aseismic creep. A high hydraulic diffusivity of about 1-10 m^2/s would be however required to account for the spatial extent of the possible interactions (~0.5-1 km) and the inter-event times (hours to days). The shallower location of the aftershocks compared to both main shocks could also point to the migration of fluids toward the surface. The occurrence of collocated events of comparable sizes and focal mechanisms, also named seismic repeaters, is often attributed to the presence of aseismic creep. But without further observations it would be difficult to support or rule out this hypothesis. Either the presence of high pore pressure or aseismic slip has important implications for the present-day earthquake potential of the VBFS to produce large earthquakes.

Das Wiener-Becken-Störungssystem (VBFS) ist eine der seismisch aktivsten Regionen Österreich. Das VBFS ist eine sinistrale Blattverschiebung, welche den südlichen Teil des Wiener Beckens durchzieht. Damit ist es Teil eines größeren Systems von Verwerfungen, welches die Nordbewegung der adriatischen Mikroplatte begleitet. Im Jahr 2000 und 2013 gab es jeweils zwei Erdbebenpaare an der VBFS, die von einer Serie an Nachbeben begleitet wurden. Die Hauptbeben ereigneten sich rund um Ebreichsdorf, einem Ort an dem schon mehrere Erdbebenserien aufgezeichnet wurden. Jedes der beiden Bebenpaare scheint praktisch am gleichen Ort stattgefunden zu haben, auch wenn hochauflösende « double-difference » Hypozentrem nur für die Beben von 2013 zur Verfügung stehen. Diese Arbeit konzentriert sich daher auf die Serie von 2013. Wir untersuchen die Wechselwirkungen zwischen den beiden Hauptbeben und ihrer 18 Nachbeben. Die beiden Hauptbeben fanden nahezu an der gleichen Stelle in einer Tiefe von 10.5 km statt, während die Nachbeben ein flaches Ellipsoid bilden, mit langer Achse parallel der Verwerfung. Wir verwenden zwei unterschiedliche Coulomb-Spannungsmodelle, um mögliche statische Spannungsübertragung zwischen den Hauptbeben und den Nachbeben zu untersuchen: das « apparent friction » Models sowie ein isotropes poroelastisches Modell. Beide Modelle liefern Coulomb-Bruchspannungsänderungen unter 0,01 MPa an den Positionen der Nachbeben. Statische Spannungsübertragung scheint deswegen eine eher unwahrscheinliche Erklärung für das Nachbebenmuster zu sein, auch wenn Wechselwirkungen zwischen den Nachbeben eine Rolle bei ihrer Auslösung spielen könnten. Zwei weitere Mechanismen werden berücksichtigt: Porendruckdiffusion entlang einer idealisierten Verwerfungsfläche sowie aseismisches Kriechen. Eine hohe hydraulische Diffusivität von etwa 1-10 m^2/s wäre jedoch im ersteren Fall erforderlich, um die räumliche Ausdehnung der möglichen Wechselwirkungen (~ 0,5-1 km) und den unterschiedlichen Intervallen (Stunden bis Tage) zu erklären. Die seichtere Lage hingegen der Nachbeben im Vergleich zu den beiden Hauptbeben steht im Einklang mit einer Migration von Fluiden in Richtung Oberfläche. Das Auftreten von Ereignissen vergleichbarer Größe und Herdmechanismus, welches als « seismic repeater » bezeichnet wird, wird oft auf das Vorhandensein von aseismischem Kriechen zurückgeführt. Ohne weitere Beobachtungen wäre es allerdings schwierig, diese Hypothese hier zu bestätigen oder auszuschließen. Die Anwesenheit von hohem Porendruck oder aseismischem Kriechen hätte wichtige Auswirkungen bzgl. des Auftretens größerer Erdbeben entlang des Störungssystems im Wiener Becken.

1. Introduction

The Vienna Basin is located at the intersection between the Eurasian plate in the North, the Pannonian Basin in the South, the Eastern Alps to the West, and the Western Carpathians to the East (e.g., Schmid et al., 2008). Considering the presentday kinematics, the Eurasian plate in this region is mainly constituted by the rigid Bohemian Massif which, together with the Adriatic microplate going northward, induce compressional stresses in the Alpine area (Grenerczy et al., 2005). This leads to the eastward extrusion of part of both the Pannonian Basin and the Eastern Alps (Gutdeutsch and Aric, 1987; Ratschbacher et al., 1991; Grenerczy et al., 2000; Brückl et al., 2010).

The extrusion is largely accommodated on the northeastern part of the Eastern Alps by strike-slip faulting (Grenerczy et al., 2005), the fault system constituting the Vienna pull-apart Basin taking an active part in this process. The southern border of the Vienna Basin, the Vienna Basin Fault System (VBFS), is in the continuation of the Mur-Mürz-Linie (MML) fault, and then joins with the extension of the Steinberg fault to the northeast of the Vienna Basin (Decker et al., 2005). The basin is filled by about 3 to 8 km of Cenozoic sediments and underpinned by the rocks of the Bohemian Massif (Reinecker and Lenhardt, 1999; Decker et al., 2005).

GPS measurements show that the MML and VBFS, which the Ebreichsdorf area belongs to, accommodate approximately 0.5 mm of displacement per year (Umnig et al., 2015). These faults are among the most actives in Austria (Hausmann et al., 2010; Lenhardt et al., 2007), with known historical seismicity up to magnitude 6 (Lenhardt et al., 2007). The relatively linear fault trace of the MML gets more complicated as it enters the Vienna Basin pull-apart system. Specifically, the Ebreichsdorf area is located in a smaller-scale pull-apart basin called the Mitterndorf Basin involving both sinistral strike slip and normal faulting (Hinsch et al., 2005).

The seismicity along the VBFS seems to concentrate in clusters which are located approximately 20 km apart, and the Ebreichsdorf region is one of them (Apoloner et al., 2015). Recently, this region experienced four earthquakes with local magnitudes greater than 4: two earthquakes of local magnitudes 4.8 and 4.5 in July 2000 (Meurers et al., 2004), and two earthquakes of local magnitude 4.2 in September and October 2013 (Figs. 1, 2) (Apoloner et al., 2014). The focal mechanisms of these events, calculated by the ZAMG (Zentralanstalt für Meteorologie und Geodynamik), are consistent with local VBFS kinematics with mechanisms mainly sinistral strike slip and a quasi-vertical fault plane oriented WSW-ENE. Both pairs of main shocks generated about 20-30 aftershocks with local magnitudes between 0.5 and 3.4. Epicentres of these aftershocks form elongated ellipsoids close to the VBFS with long-axes parallel to the

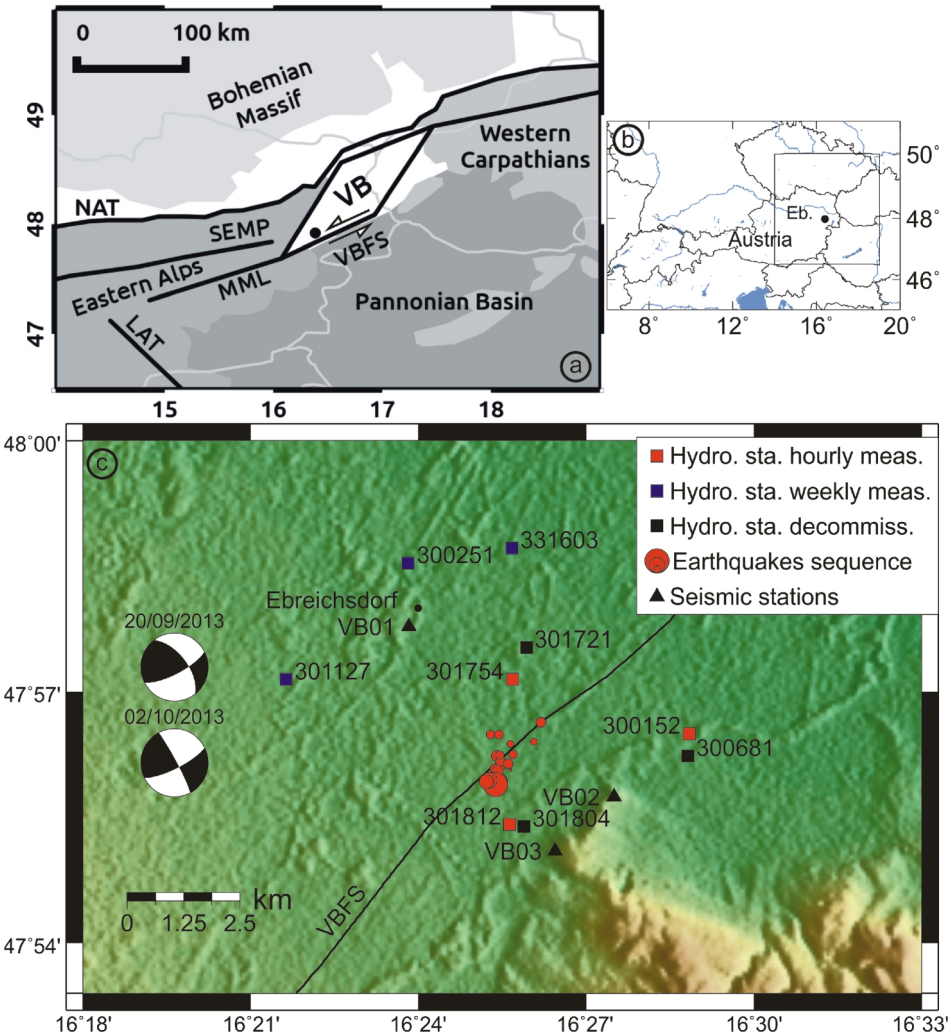

Figure 1: (a) Schematic tectonic settings around the Vienna basin (VB) modified after Brückl et al. (2010), showing the main faults and tectonic units. Light gray lines indicate country borders, and the black dot the position of Ebreichsdorf area. The position of this map is shown by the inset (b). Abbreviations: NAT, North Alpine Thrust fault; SEMP, Salzachtal-Ennstal-Mariazell–Puchberg fault; MML, Mur-Mürz-Linie fault; LAT, Lavant fault; VBFS: Vienna Basin Fault System. (c) Zoom in the area of Ebreichsdorf, showing the aftershock sequence of 2013 (red dots with sizes proportional to their local magnitude), the three temporary seismic stations deployed close to the sequence to record the aftershock sequence after the second main shock (black triangles), and the location of hydrological stations used to investigate potential hydrological manifestations related to the earthquake sequence (squares, see Appendix A). The focal mechanisms by Hausmann et al. (2014) of both main shocks are shown on the left, and the black line indicates the idealized trace of the VBFS.

main fault trace (Apoloner et al., 2015).

In the case of the Ebreichsdorf sequence in 2013, high-precision double-difference locations show that the main shocks are collocated within the location uncertainties (Apoloner et al., 2015). Whether they share or not the same fault plane cannot be resolved due to the uncertainties in the locations and focal mechanisms. The occurrence of collocated pairs of main shocks of similar magnitudes is unexpected because the first main shock should have released the tectonic stresses that had build-up at its location. This raises the question of possible interactions between the earthquakes of this sequence, and if particular mechanisms such as high-pressured fluids or aseismic creep could be at play in this region. This in turn has some wider implications on the potential seismic hazard associated with the VBFS in Ebreichsdorf area.

After reviewing some obser-vations from the Ebreichsdorf 2013 sequence, we will investigate possible earthquakes interactions using the Coulomb stress transfer model (e.g., King et al., 1994; Toda et al., 1998) using the apparent friction and isotropic poroelastic models (Harris, 1998; Cocco and Rice, 2002). We will then discuss observations and model results in terms of potential interpretations for the occurrence of these sequences in Ebreichsdorf area.

2. Ebreichsdorf sequence in 2013

The 1st main shock of the Ebreichsdorf sequence in 2013 occurred on September 20, 2013. This event has a local magnitude of 4.2 and was widely felt throughout Eastern Austria, similarly to the 2000 earthquakes (Meurers et al., 2004). Its focal mechanism shows a sinistral strike-slip fault oriented N63 and strongly dipping toward the SE (73°), which is consistent with the orientation of the VBFS in the area (Fig. 1). This event was followed by 3 events the same day, and by 10 in total before the 2nd main event.

The 2nd main shock, which occurred on October 2, 2013, has very similar local magnitude and focal mechanism compared to the 1st main event (Fig. 1). This event was preceded by an acceleration of the seismicity rate with 4 events occurring earlier the same day. They could actually either correspond to aftershocks from the 1st event or foreshocks to the 2nd, even though these events were located shallower and further to the northeast. The 2nd event was then followed by 8 events with the last one occurring on September 23, 2013. The complete aftershocks sequence consists of 18 events with local magnitudes between 1 and 3. These events seem to delineate a plane above the two main shocks which follows the presumed trace of the VBFS in this area (Figs. 1, 2).

Owing to the high waveforms similarity of the earthquakes of this sequence, Apoloner et al., (2015) relocated them using catalog and cross-correlation data with the double-difference algorithm HypoDD (Waldhauser and Ellsworth, 2000). The velocity model used is a 3D velocity model for P-waves and S-waves of Eastern Austria (Behm et al., 2007a, 2007b). In the following we use this relocated set of locations. Noticeably, the two main shocks are collocated within the location uncertainties (Fig. 2). Their waveforms are indeed very similar (Fig. 3). The discrepancy in their spectra in Figure 3b is reversed whether we consider a station to the NE (RNSA) or SW (RWNA) of the events. This indicates that the difference in frequency between the two events most likely arises from directivity effects.

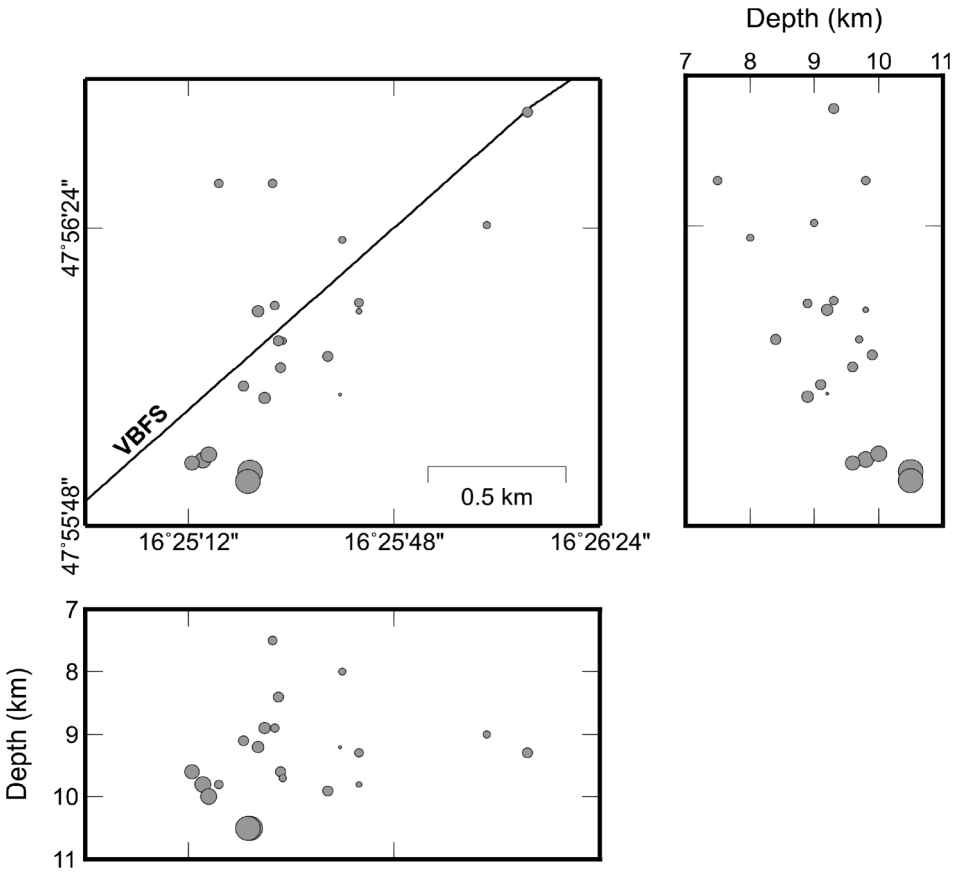

Figure 2: Zoomed view of the 2013 Ebreichsdorf earthquakes sequence (gray dots with sizes proportional to their local magnitude). VBFS: Vienna Basin Fault System (black line).

The reader is referred to Apoloner et al. (2014) and Apoloner et al. (2015) for more details on the location procedure, a complete list of the stations used to locate these events, as well as their exact timing and locations.

3. Coulomb stress interactions

Static stress changes calculated for large earthquakes seem to be correlated with the pre-

sence or absence of aftershocks (King et al., 1994; Toda et al., 1998). Areas exhibiting an increase in static stress are brought closer to failure and show higher aftershock activities, and the opposite for areas of static stress decrease (also called stress shadows). Static stress loading from previous earthquakes is also invoked to explain the triggering of nearby earthquakes, such as in the case of the 20th century sequence of large earthquakes along the North Anatolian fault in Turkey (Stein et al., 1997).

These calculations are based on the change in Coulomb failure stress on a predefined fault plane, incorporating the effective stress principle (e.g., Beeler et al., 2000; Jaeger et al., 2007), given by

$$\Delta\sigma_c = \Delta\tau_s - \mu(\Delta\sigma_n - \Delta\rho) \quad (1)$$

where $\Delta\sigma_c$ is the change in Coulomb failure stress, $\Delta\tau_s$ is the change in shear stress on the fault plane in the slip direction, μ is the friction coefficient, $\Delta\sigma_n$ is the change in fault-normal stress (positive for fault unclamping), and Δp is the change in pore pressure. Failure occurs on a given fault plane when $\Delta\sigma_c$ reaches a certain threshold which is unknown as in-situ background stresses on fault planes are generally also unknown. Strain, shear and normal stresses due to the earthquake are calculated using the dislocation model of Okada (1992).

Pore-pressure distribution prior to the earthquake will influence the change in Coulomb failure stress. Coseismic stresses typically act on timescales of seconds, generally much shorter than the timescale of pore-pressure diffusion in the medium (Cocco and Rice, 2002; Manga and Wang, 2007). In consequence, during coseismic stresses variations, the medium is considered to be in "undrained" conditions which means that no fluid flow takes place (Rice and Cleary, 1976). In the case of an isotropic poroelastic material in undrained conditions, the pore-pressure variations Δp are related to the change in mean stress through the Skempton coefficient B as

$$\Delta\rho = B\frac{\Delta\sigma_{kk}}{3} \quad (2)$$

where $\Delta\sigma_{kk}$ is the sum of the changes in stress components corresponding to the trace of the stress tensor. Values for the Skempton coefficients range from 0.5 to 0.9 for consolidated rocks and up to 1 for unconsolidated materials (Cocco and Rice, 2002, and references therein). Using Eq. 2, the Coulomb failure stress becomes

$$\Delta\sigma_c = \Delta\tau_s - \mu\left(\Delta\sigma_n - B\frac{\Delta\sigma_{kk}}{3}\right) \quad (3)$$

In the following, we refer to this equation as the isotropic model. Many authors assume that the mean stress can be replaced by the fault-normal stress (e.g., Stein et al., 1992; Harris et al., 1995; Toda et al., 1998), which would be appropriate for fault zones with strong fault-parallel anisotropy (Cocco and Rice, 2002), simplifying Eq. 3 to

$$\Delta\sigma_c = \Delta\tau_s - \mu'\Delta\sigma_n \quad (4)$$

with the apparent friction coefficient $\mu' = \mu(1-B)$.

These simple Coulomb failure stress models have some limitations in common. They consider a homogeneous medium with the fault zone having the same properties as the surrounding medium (Cocco and Rice, 2002). The static stress changes calculated are generally small, on the order of 0.1 MPa (Harris, 1998), compared to the stress drop of earthquakes (~1 – 10 MPa; Stein and Wyssession, 2003). Interpretations based in these models are then mainly qualitative in terms of areas where failure is promoted or delayed. In addition, uncertainties in fault parameters typically coming from focal mechanisms (i.e. fault strike, dip and rake) and the complexity of slip patterns are not taken into account in most cases but could be essential (Kilb et al., 1997; Hardebeck et al., 1998). For the Coulomb stress modelling, we here consider undrained conditions where the pore pressure diffusion is not taken into account, even though this might not be appropriate for the timescales of the Ebreichsdorf sequence (Jónsson et al., 2003).

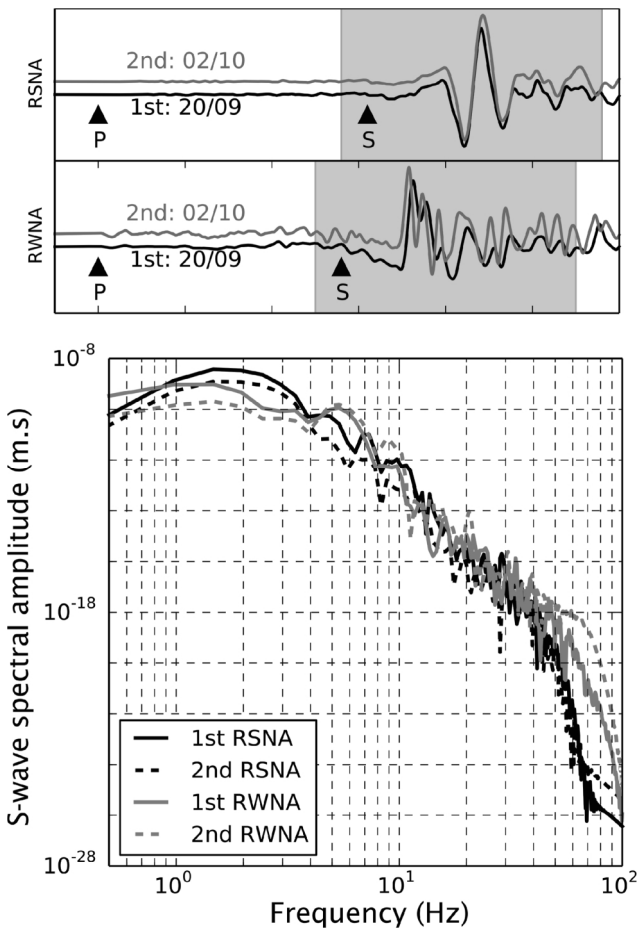

Figure 3: Normalized seismic traces of the first and second main shock of the 2013 Ebreichsdorf sequence (top, instruments response removed), and displacement spectra corresponding to the part of the S-wave in these traces (bottom) indicated by the grey area, for two stations located approximately 20 km away from the two main shocks. RSNA is located 20 km to the NE, while RWNA is located 20 km to the SW. The seismic traces are aligned on the P-wave arrival times; P- and S-wave arrivals are indicated by black arrows. Note the high similarity in waveforms and frequency content of the two main events. At these stations, their corner frequencies are in the range 3-6 Hz.

4. Parameters and results

Calculations of Coulomb stress changes are made with the Coulomb 3.3 software (Lin and Stein, 2004; Toda et al., 2005) for both the apparent friction and isotropic models. The main parameters used are an apparent friction coefficient μ' of 0.35, corresponding to a typical friction coefficient μ of 0.7 (Byerlee, 1978) and a Skempton coefficient B of 0.5, a Young modulus of 75 GPa and a Poisson ratio of 0.25 (Stein and Wyssession, 2003). Regional stresses correspond to a strike-slip system with the maximum and minimum compressive principal stresses being horizontal, and oriented N220 and N130, respectively (Bada et al., 2007).

The fault orientations of the first and second main event, which correspond to the source and receiver faults in the Coulomb failure stress calculations, are extracted from their focal mechanisms (Fig. 1). For the source and receiver faults, the strike/dip/rake sets are 62.5/73.3/31.2 and 63.3/76/5.3 degrees, respectively. Their geometries are estimated using their local magnitude (4.2), corner frequencies (1-6 Hz, Fig. 3) and scaling relationships (Geller, 1976; Madariaga, 1976; Stein and Wyssession, 2003). Both faults have a length of 500 m and a width of 250 m, the second main event being approximately 40 m to the SE of the first main event. The source fault also has an average slip of 3.6 cm in the rake direction. The stress perturbations are calculated for the first main event, assuming receiver faults with the geometry of the second main event (Fig. 4). Calculations using receiver faults with the geometry of the first event gives similar results as both main events have similar local magnitudes and focal mechanisms.

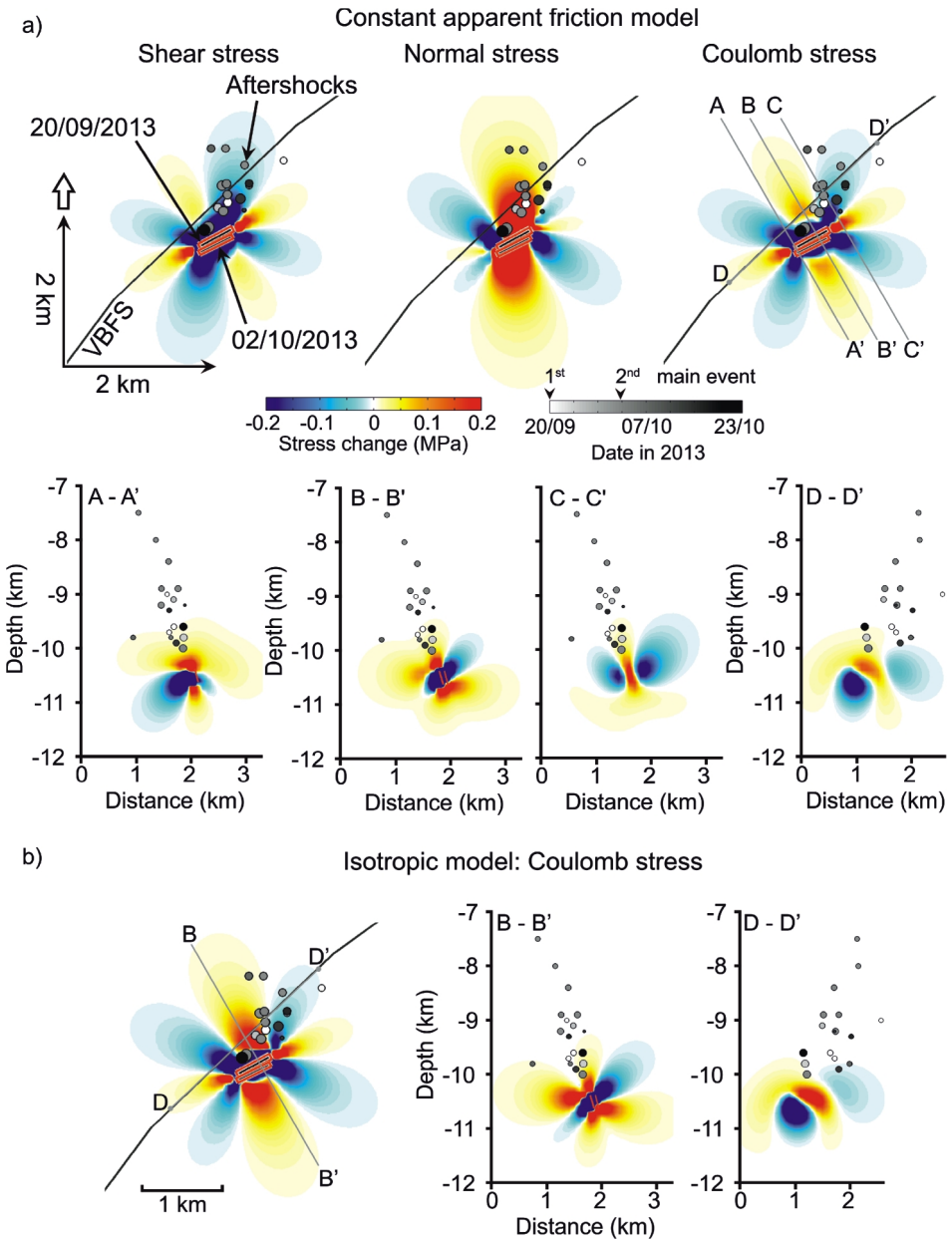

Figure 4: a) Changes in Coulomb failure stress due to the first main event using the constant apparent friction model ($\mu' = 0.35$, see text for remaining parameters), calculated on faults with the orientation of the second main event. On top, changes in shear, normal and Coulomb stresses are shown on the left, middle and right, respectively (in map view). The locations of the four vertical cross-sections across the Coulomb stress change map are indicated by the gray lines. b) Changes in Coulomb failure stress due to the first main event using the isotropic model ($\mu = 0.7$ and $B = 0.5$, see text for remaining parameters), calculated on faults with the orientation of the second main event (left). For comparison with the apparent friction model, two vertical cross-sections at the same locations are shown on the right. Positive stress changes are indicated by warm colors while negative changes are indicated by cold colors. Main shocks are indicated by red rectangles, aftershocks by dots with sizes proportional to their local magnitude and grey-coded depending on their occurrence time, and the VBFS by the black line.

Considering changes in shear and Coulomb stresses for the apparent friction model, the second main event is located within the stress shadow of the first event (Fig. 4a). It is however partially in the zone of normal stress increase (unclamping). The aftershocks are located above the two main shocks and, except for one, in areas of positive Coulomb failure stress changes mainly due to shear stress increase (Figs. 4, 5). However, for most events these changes are very small, lower than 0.01 MPa (Fig. 5). In our configuration, the results using the isotropic model are relatively similar to those of the apparent friction model (Figs. 4, 5). The influence of the normal stress is more important in the

isotropic model for most events, reducing the Coulomb failure stress changes.

Changes in Coulomb failure stress seem then insufficient to be the cause of the aftershocks, even though very small changes on the order of 0.01 MPa have sometimes been used to explain the triggering of aftershocks (e. g., King et al., 1994). One alternative hypothesis would be that the aftershocks triggered each other in a cascade-like fashion. We will discuss further potential mechanisms below.

5. Discussion

Static stress triggering of the aftershocks due to coseismic static stress transfer from the first main event seems unlikely because of the small amplitude of Coulomb stress changes at the location of the aftershocks (Fig. 5). This is also unlikely for the second main event due to its occurrence in the stress shadow coming from the first main event. On the other hand, the first main event might have released only a part of the stress accumulated on this portion of the fault (Hinsch and Decker, 2003), leaving the possibility for this asperity to produce another event. This would be possible especially if dynamic stress effects have caused a reduction in fault strength (friction coefficient), for instance related to the weakening effects of earthquakes that can be observed seismologically (e.g., Baisch and Bokelmann, 1991). However, the recent geodetic measurements by Unmig et al. (2015) seem to indicate that the strain accumulated in the area is small in comparison with the cumulated coseismic displacements. In addition, coseismic slip and stress drop distributions on the rupture plane are not homogeneous, producing areas where stress is increased or decreased (Bouchon, 1997; Sammis et al., 1999). This complex pattern in Coulomb stress changes is not taken into account in our model which assumes a homogeneous slip on the fault plane.

The b-value is another interesting parameter corresponding to the slope of cumulative earthquake magnitude distributions expressed through the Gutenberg-Richter power law (Gutenberg and Richter, 1944). This parameter seems correlated to the local differential stress state (Scholz, 2015) and could reveal potential highly stressed patches (Schorlemmer and Wiemer, 2005). This has implications for seismic hazard and the location of aftershocks, such as for those of the Ebreichsdorf sequence, as the seismicity would primarily be associated with these patches.

If the first main event caused the second one, then the response from the disturbance coming from the first main event would have been delayed by 12 days. This would imply some in-situ relaxation mechanism, potentially involving fluid diffusion in the surroundings of the first main event, as both events are located very close to each other. Coseismic stress variations in the ground induce pore pressure re-adjustments on longer timescales (e.g., Nur and Booker, 1972; Roeloffs, 1998; Jónsson et al., 2003). For an isotropic poroelastic material, an order of magnitude of the timescale of pore pressure diffusion is given by $t \sim L^2/D$ (Manga and Wang, 2007), where L is the spatial scale of pore pressure diffusion and D

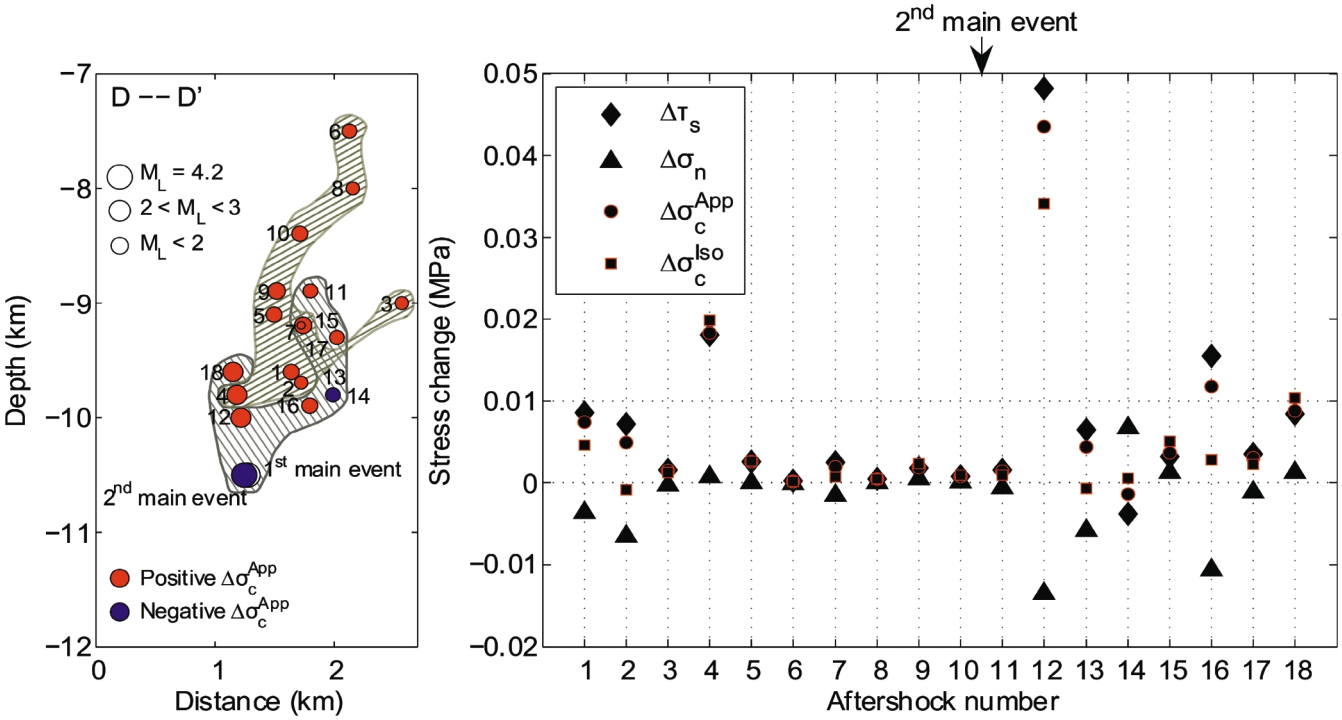

Figure 5: (Right) Changes in shear $\Delta\tau_s$, normal $\Delta\sigma_n$ and Coulomb stress using the constant apparent friction $\Delta\sigma_c^{App}$ and isotropic $\Delta\sigma_c^{Iso}$ models, at the location of the aftershocks. The aftershocks are numbered in chronological order. (Left) Vertical cross-section along the strike of the VBFS with the complete aftershock sequence projected on it (see Fig. 4 for location of cross-section D-D'). The size of earthquake symbols is proportional to their local magnitude M_L. They are color-coded according to the polarity of the change in $\Delta\sigma_c^{App}$. The two gray hatched patches delimit the locations of the main shocks with the first 10 aftershocks, and the next 8 aftershocks.

is the hydraulic diffusivity.

During the Ebreichsdorf 2013 sequence, inter-event distances of few hundred meters to one kilometer and inter-event periods of hours to days would be compatible with an average hydraulic diffusivity of about 1-10 m^2/s This would correspond to a highly permeable material (Roeloffs et al., 2003; Manga and Wang, 2007) and is few orders of magnitudes higher than values of hydraulic diffusivities found for fault gouges (10^{-2} – 10^{-7} m^2/s; Wibberley, 2002; Doan et al., 2006).

Fluid overpressure at depth could also be the cause of this high diffusivity, due to the non-linear relationship between pore pressure and hydraulic diffusivity (Miller et al., 2004; Hummel and Müller, 2009). If pore pressure diffusion is the driving mechanisms of this sequence, it could explain the position of the aftershocks above the main shocks with the propagation of fluids toward the surface. The first part of the sequence, before the second main event, seems to migrate toward the surface, whereas the second part seems to envelope the area delimited by the events of the first part. However, no unambiguous correlation between hydrological measurements on the surface and the spatio-temporal distribution of this sequence has been found (see Appendix A).

The near-collocation of two main events of similar magnitudes is essentially similar in character to seismic repeaters (e. g., Chen et al., 2013). Beside coseismic stresses (Nadeau et al., 1995) and fluid overpressure (Daniel et al., 2011), a third alternative explanation is invoked with the presence of aseismic creep in the area surrounding these kind of events, re-loading the same asperity (Bouchon et al., 2011). Aseismic creep seems to take place also on portions of other continental strike-slip faults, such as the San Andreas fault (Gratier et al., 2011 and references therein) and the North Anatolian fault (Bouchon et al., 2011; Çakir et al., 2012). The actual presence of aseismic slip on the VBFS could be investigated using different kind of instrumentation, dense GPS network, InSAR and extensometers for surface deformation, and broad-band seismometers to better characterize the seismicity of this area. Comparison between long-term historical seismicity and the strain rate in the VBFS would also be helpful for detecting deficits in seismic strain in the area that could be accounted for by aseismic creep or forthcoming events (Hinsch and Decker, 2003). The presence or not of aseismic creep and over pressurized fluids in the VBFS has wider implications on potential seismic hazards in this region, i.e., on the timing of future ruptures and their spatial extension.

6. Conclusion

The Ebreichsdorf area is located along the VBFS, one of the most seismically active region of Austria. At this location, two sequences with similar characteristics occurred in 2000 and 2013: one main shock was followed by aftershocks, then by another main shock and further aftershocks. High-resolution locations are available for the sequence in 2013, showing that the two main shocks are collocated at depth within the uncertainties in locations, while the aftershocks are shallower and seem to follow the orientation of the VBFS in the area.

Using Coulomb failure stress modeling, we show that Coulomb stress transfer from the two main shocks seem insufficient to explain the triggering of the aftershocks. Both the apparent friction model and the isotropic model present coseismic static stress changes of less than 0.01 MPa for most aftershocks. The sequence could then be driven by other mechanisms such as dynamic effects reducing fault strength, high pore-pressure at depth, which could explain the spatio-temporal distribution of the events despite the necessity for a high hydraulic diffusivity, or aseismic creep, which is frequently invoked as a cause for seismic repeaters. The presence of some of these mechanisms along the VBFS would have important implications for the seismic hazard of this region; the VBFS having the potential of generating magnitude 6 earthquakes.

Acknowledgments

We thank the ZAMG, the Technical University of Vienna, ORFEUS and GeoRisk Earthquake Engineering for providing the seismic data and the focal mechanisms of the 2013 Ebreichsdorf sequence, the Hydrological Survey of Lower Austria for providing the time series of the hydrological stations around Ebreichsdorf, and M. Ristic and M. Dorninger for providing the precipitation data from the ZAMG. We thank Ewald Brückl and an anonymous reviewer for their useful comments which helped improve the original manuscript. The Generic Mapping Tools (GMT) software from Wessel and Smith (2013) has been used to plot parts of Figs. 1 and 2.

References

Apoloner, M.-T., Tary, J. B. and Bokelmann, G., 2015. The 2013 Earthquake series: Relative Location. Austrian Journal of Earth Sciences, 108/2, this volume. http://dx.doi.org/

Apoloner, M.-T., Bokelmann, G., Bianchi, I., Brückl, E., Hausmann, H., Mertl, S. and Meurers, R., 2014. The 2013 earthquake series in the Southern Vienna Basin: location. Advances in Geosciences, 36, 77-80. http://dx.doi.org/10.5194/adgeo-36-77-2014

Bada, G., Horváth, F., Dövényi, P., Szafián, P., Windhoffer, G. and Cloetingh, S., 2007. Present-day stress field and tectonic inversion in the Pannonian basin. Global and Planetary Change, 58, 165-180. http://dx.doi.org/10.1016/j.gloplacha.2007.01.007

Baisch, S. and Bokelmann, G.H.R., 2001. Seismic waveform attributes before and after the Loma Prieta earthquake: Scattering change near the earthquake and temporal recovery. Journal of Geophysical Research, 106, 16323-16338. http://dx.doi.org/10.1029/2001JB000151

Beeler, N.M., Simpson, R.W., Hickman, S.H. and Lockner, D.A., 2000. Pore fluid pressure, apparent friction, and Coulomb failure. Journal of Geophysical Research, 105(B11), 25533-25542. http://dx.doi.org/10.1029/2000JB900119

Behm, M., Brückl, E., Chwatal, W. and Thybo, H., 2007a. Application of stacking and inversion techniques to three-dimen-

sional wide-angle reflection and refraction seismic data of the Eastern Alps. Geophysical Journal International, 170, 275-298. http://dx.doi.org/10.1111/j.1365-246X.2007.03393.x

Behm, M., Bruckl, E. und Mitterbauer, U., 2007b. A New Seismic Model of the Eastern Alps and its Relevance for Geodesy and Geodynamics. VGI Österrreichische Zeitschrift für Vermessung & Geoinformation, 2, 121-133.

Bouchon, M., 1997. The state of stress on some faults of the San Andreas System as inferred from near-field strong motion data. Journal of Geophysical Research, 102(B6), 11731-11744. http://dx.doi.org/10.1029/97JB00623

Bouchon, M., Schmittbuhl, J., Karabulut, H. and Bouin, M.-P., 2011. Extended Nucleation of the 1999 Mw 7.6 Izmit Earthquake. Science, 331, 877-880. http://dx.doi.org/10.1126/science.1197341

Brückl, E., Behm, M., Decker, K., Grad, M., Guterch, A., Keller, G.R. and Thybo, H., 2010. Crustal structure and active tectonics in the eastern Alps. Tectonics, 29, TC2011. http://dx.doi.org/10.1029/2009TC002491

Byerlee, J., 1978. Friction of rocks. Pure and Applied Geophysics, 116, 615-626.

Çakir, Z., Ergintav, S., Özener, H., Dogan, U., Akoglu, A. M., Meghraoui, M. and Reilinger, R., 2012. Onset of aseismic creep on major strike-slip faults. Geology, 40, 1115-1118. http://dx.doi.org/10.1130/G33522.1

Chen, K.H., Bürgmann, R. and Nadeau, R.M., 2013. Do earthquakes talk to each other? Triggering and interaction of repeating sequences at Parkfield. Journal of Geophysical Research, 118, 165–182. http://dx.doi.org/10.1029/2012JB009486

Cocco, M. and Rice, J.R., 2002. Pore pressure and poroelasticity effects in Coulomb stress analysis of earthquake interactions. Journal of Geophysical Research, 107(B2). http://dx.doi.org/10.1029/2000JB000138

Daniel, G., Prono, E., Renard, F., Thouvenot, F., Hainzl, S., Marsan, D., Helmstetter, A., Traversa, P., Got, J.L., Jenatton, L. and Guiguet, R., 2011. Changes in effective stress during the 2003-2004 Ubaye seismic swarm, France. Journal of Geophysical Research, 116, B01309. http://dx.doi.org/10.1029/2010JB007551

Decker, K., Peresson, H. and Hinsch, R., 2005. Active tectonics and Quaternary basin formation along the Vienna Basin Transform fault. Quaternary Science Reviews, 24, 307-322. http://dx.doi.org/10.1016/j.quascirev.2004.04.012

Doan, M.L., Brodsky, E.E., Kano, Y. and Ma, K.F., 2006. In situ measurement of the hydraulic diffusivity of the active Chelungpu Fault, Taiwan. Geophysical Research Letters, 33, L16317. http://dx.doi.org/10.1029/2006GL026889

Gratier, J.-P., Richard, J., Renard, F., Mittempergher, S., Doan, M.-L., Di Toro, G., Hadizadeh, J. and Boullier, A.-M., 2011. Aseismic sliding of active faults by pressure solution creep: Evidence from the San Andreas Fault Observatory at Depth. Geology, 39, 1131-1134. http://dx.doi.org/10.1130/G32073.1

Geller, R.J., 1976. Scaling relations for earthquake source parameters and magnitudes. Bulletin of the Seismological Society of America, 66(5), 1501-1523.

Grenerczy, G., Kenyeres, A. and Fejes, I., 2000. Present crustal movement and strain distribution in Central Europe inferred from GPS measurements. Journal of Geophysical Research, 105(B9), 21835-21846. http://dx.doi.org/10.1029/2000JB900127

Grenerczy, G., Sella, G., Stein, S. and Kenyeres, A., 2005. Tectonic implications of the GPS velocity field in the northern Adriatic region. Geophysical Research Letters, 32, L16311. http://dx.doi.org/10.1029/2005GL022947

Gutdeutsch, R. and Aric, K., 1987. Tectonic block models based on the seismicity in the east Alpine–Carpathians and Pannonian area. In: H.W. Flügl and P. Faupl (eds.), Geodynamics of the Eastern Alps. F. Deuticke, Vienna, pp. 309–324.

Gutenberg, B. and Richter, C.F., 1944. Frequency of earthquakes in California, Bulletin of the Seismological Society of America, 34, 185-188.

Hardebeck, J.L., Nazareth, J.J. and Hauksson, E., 1998. The static stress change triggering model: Constraints from two southern California aftershock sequences. Journal of Geophysical Research, 103(B10), 24427-24437.

Harris, R.A., 1998. Introduction to Special Section: Stress Triggers, Stress Shadows, and Implications for Seismic Hazard. Journal of Geophysical Research, 103(B10), 24347-24358.

Harris, R.A., Simpson, R.W. and Reasenberg, P.A., 1995. Influence of static stress changes on earthquake locations in southern California. Nature, 375, 221-224.

Hausmann, H., Hoyer, S., Schurr, B., Brückl, E., Houseman, G. and Stuart, G., 2010. New Seismic Data improve earthquake location in the Vienna Basin Area, Austria. Austrian Journal of Earth Sciences, 103/2, 2-14.

Hausmann, H., Meurers, R. and Horn, N., 2014. The 2013 Earthquakes in the Vienna Basin: Results from strong-motion and macroseismic data. Second European Conference on Earthquake Engineering and Seismology, Istanbul, Turkey.

Hinsch, R. and Decker, K., 2003. Do seismic slip deficits indicate an underestimated earthquake potential along the Vienna Basin Transfer Fault System?. Terra Nova, 15, 343-349. http://dx.doi.org/10.1046/j.1365-3121.2003.00504.x

Hinsch, R., Decker, K. and Wagreich, M., 2005. 3-D mapping of segmented active faults in the southern Vienna Basin. Quaternary Science Reviews, 24, 321-336. http://dx.doi.org/10.1016/j.quascirev.2004.04.011

Hummel, N. and Müller, T.M., 2009. Microseismic signatures of non-linear pore-fluid pressure diffusion. Geophysical Journal International, 179, 1558-1565. http://dx.doi.org/10.1111/j.1365-246X.2009.04373.x

Jaeger, J.C., Cook, N.G. W. and Zimmerman, R.W., 2007. Fundamentals of Rock Mechanics. 4th Ed., Blackwell Publishing, MA, USA, pp. 475.

Jónsson, S., Segall, P., Pedersen, R. and Björnsson, G., 2003. Post-earthquake ground movements correlated to pore-pressure transients. Nature, 424, 179-183. http://dx.doi.org/10.1038/nature01776

Kilb, D., Ellis, M., Gomberg, J. and Davis, S., 1997. On the origin of diverse aftershock mechanisms following the 1989 Loma Prieta earthquake. Geophysical Journal International 128(3), 557-570.

King, G.C.P., Stein, R.S. and Lin, J., 1994. Static Stress Changes and the Triggering of Earthquakes. Bulletin of the Seismological Society of America, 84(3), 935-953.

King, C.-Y., Azuma, S., Igarashi, G., Ohno, M., Saito, H. and Wakita, H., 1999. Earthquake-related water-level changes at 16 closely clustered wells in Tono, central Japan. Journal of Geophysical Research, 104(B6), 13073-13082.

Lenhardt, W., Švancara, J., Melichar, P., Pazdírková, J., Havíř, J. and Sýkorová, Z., 2007. Seismic activity of the Alpine-Carpathian-Bohemian Massif region with regard to geological and potential field data. Geologica Carpathica, 58(4), 397-412.

Lin, J. and Stein, R.S., 2004. Stress triggering in thrust and subduction earthquakes and stress interaction between the southern San Andreas and nearby thrust and strike-slip faults. Journal of Geophysical Research, 109, B02303. http://dx.doi.org/10.1029/2003JB002607

Madariaga, R., 1976. Dynamics of an expanding circular fault. Bulletin of the Seismological Society of America, 66(3), 639-666.

Manga, M. and Wang, C.-Y., 2007. Earthquake hydrology. In: G. Schubert (ed.), Treatise on Geophysics, 4, Elsevier, Amsterdam, 293-320. http://dx.doi.org/10.1016/B978-044452748-6.00074-2

Manga, M., Beresnev, I., Brodsky, E.E., Elkhoury, J.E., Elsworth, D., Ingebritsen, S.E., Mays, D.C. and Wang, C.-Y., 2012. Changes in permeability caused by transient stresses: Field observations, experiments, and mechanisms. Reviews of Geophysics, 50, RG2004. http://dx.doi.org/10.1029/2011RG000382

Meurers, R., Lenhardt, W., Leichter, B. and Fiegweil, E., 2004. Macroseismic Effects of the Ebreichsdorf Earthquake of July 11, 2000 in Vienna. Austrian Journal of Earth Sciences, 95/96, 20-27.

Miller, S.A., Collettini, C., Chiaraluce, L., Cocco, M., Barchi, M. and Kaus, B.J.P., 2004. Aftershocks driven by a high-pressure CO_2 source at depth. Nature, 427, 724-727. http://dx.doi.org/10.1038/nature02251

Nadeau, R.M., Foxall, W. and McEvilly, T.V., 1995. Clustering and Periodic Recurrence of Microearthquakes on the San Andreas Fault at Parkfield, California. Science, 267, 503-507.

Nur, A. and Booker, J.R., 1972. Aftershocks caused by pore fluid flow?. Science, 175, 885-887.

Okada, Y., 1992. Internal deformation due to shear and tensile faults in a half-space. Bulletin of the Seismological Society of America, 82, 1018-1040.

Ratschbacher, L., Frisch, W., Linzer, H.-G. and Merle, O., 1991. Lateral extrusion in the eastern Alps, Part 2: Structural analysis. Tectonics 10(2), 257-271.

Reinecker, J. and Lenhardt, W.A., 1999. Present-day stress field and deformation in eastern Austria. International Journal of Earth Sciences, 88, 532-550.

Rice, J.R. and Cleary, M.P., 1976. Some basic stress diffusion solutions for fluid-saturated elastic porous media with compressible constituents. Reviews of Geophysics and Space Physics, 14(2), 227-241. http://dx.doi.org/10.1029/RG014i002p00227

Roeloffs, E.A., 1998. Persistent water level changes in a well near Parkfield, California, due to local and distant earthquakes. Journal of Geophysical Research, 103, 869-889.

Roeloffs, E., Sneed, M., Galloway, D.L., Sorey, M.L., Farrar, C.D., Howle, J.F. and Hughes, J., 2003. Water-level changes induced by local and distant earthquakes at Long Valley caldera, California. Journal of Volcanology and Geothermal Research, 127, 269-303. http://dx.doi.org/10.1016/S0377-0273(03)00173-2

Sammis, C.G., Nadeau, R.M. and Johnson, L.R., 1999. How strong is an asperity?. Journal of Geophysical Research, 104(B5), 10609-10619.

Schmid, S.M., Bernoulli, D., Fügenschuh, B., Matenco, L., Schaefer, S., Schuster, R., Tischler, M. and Ustaszewski, K., 2008. The Alpine-Carpathian-Dinaridic orogenic system: correlation and evolution of tectonic units. Swiss Journal of Geosciences, 101, 139-183. http://dx.doi.org/10.1007/s00015-008-1247-3

Scholz, C.H., 2015. On the stress dependence of the earthquake b value. Geophysical Research Letters, 42, 1399-1402. http://dx.doi.org/10.1002/2014GL062863

Schorlemmer, D. and Wiemer, S., 2005. Microseismicity data forecast rupture area. Nature, 434, 1086. http://dx.doi.org/10.1038/4341086a

Stein, R.S., Barka, A.A. and Dieterich, J.H., 1997. Progressive failure on the North Anatolian fault since 1939 by earthquake stress triggering. Geophysical Journal International, 128, 594-604.

Stein, R.S., King, G.C.P. and Lin, J., 1992. Change in failure stress on the southern San Andreas fault system caused by the 1992 Magnitude=7.4 Landers earthquake. Science, 258, 1328-1332.

Stein, S. and Wysession, M., 2003. An Introduction to Seismology, Earthquakes, and Earth Structure, Wiley, Hoboken, NJ, USA, pp. 512.

Toda, S., Stein, R.S., Reasenberg, P.A., Dieterich, J.H. and Yoshida, A., 1998. Stress transferred by the 1995 Mw = 6.9 Kobe, Japan, shock: Effect on aftershocks and future earthquake probabilities. Journal of Geophysical Research, 103(B10), 24543-24565.

Toda, S., Stein, R.S., Richards-Dinger, K. and Bozkurt, S.B., 2005. Forecasting the evolution of seismicity in southern California: Animations built on earthquake stress transfer. Journal of Geophysical Research, 110, B05S16. http://dx.doi.org/10.1029/2004JB003415

Umnig, E., Brückl, E., Maras, J. and Weber, R., 2015. Monitoring tectonic processes in Eastern Austria based on GNSS-derived site velocities. Vermessung & Geoinformation, 103(2-3/15), 198-207.

Waldhauser, F. and Ellsworth, W.L., 2000. A double-difference earthquake location algorithm: Method and application to the northern Hayward fault. Bulletin of the Seismological Society of America, 90, 1353-1368.

Wessel, P., Smith, W.H.F., Scharroo, R., Luis, J. and Wobbe, F., 2013. Generic Mapping Tools: Improved Version Released, EOS Trans. AGU, 94(45), 409-410. http://dx.doi.org/10.1002/2013EO450001

Wibberley, C.A.J., 2002. Hydraulic diffusivity of fault gouge zo-

nes and implications for thermal pressurization during seismic slip. Earth Planet Space, 54, 1153-1171. http://dx.doi.org/10.1186/BF03353317

Received: 2 February 2015
Accepted: 20 September 2015

Jean Baptiste TARY[1)2)], Maria-Theresia APOLONER[1)] & Götz BOKELMANN[1)*)]

[1)] Department of Meteorology and Geophysics, University of Vienna, Althanstrasse 14, 1090 Wien, Austria;

[2)] Department of Physics, University of Alberta, 8440 - 112 St, Edmonton, Alberta T6G 2R7, Canada;

[*)] Corresponding author, goetz.bokelmann@univie.ac.at